International Journal of Engineering & Technology, 7 (3.29) (2018) 293-300

International Journal of Engineering & Technology

Website: www.sciencepubco.com/index.php/IJET

Research paper

Torque and pitch control for wind energy conversion system using sliding mode approach

C. Subba Rami Reddy [1] *, Pedda Suresh Ogeti [2], D. Gireesh Kumar [1], N. Bhoopal [1]

[1] EEE department, B.V. Raju Institute of Technology, Narsapur, Medak, Telangana
[2] EEE department, Hyderabad Institute of Technology and Management, Hyderabad, Telangana
**Corresponding author E-mail: csubbaramireddy2020@gmail.com*

Abstract

The integration of wind energy with the grid is one of the major challenges as the wind energy depends upon the most fluctuating wind speeds. Therefore it requires a stringent methodology to control and maintain the stability of power system. This paper presents the torque and pitch control of Wind Energy Conversion System (WECS) that implements the variable speed Doubly Fed Induction Generator (DFIG) using Sliding Mode (SM) approach. For the speeds above the rated wind velocity, pitch control technique has been implemented and below the base speed torque control technique has been applied. The limitations of pitch actuator are compensated by the torque control of induction generator. The modeling and simulation of WECS with sliding mode control (SMC) scheme is carried out using MATLAB SIMULINK environment. The performance parameters such as pitch angle, active power, reactive power and rotor speed are compared for the Proportional plus Integral (PI), Linear Parameter Varying (LPV) and SMC schemes. Simulation results confirm that the performance of SM control is superior in terms of pitch, speed, active and reactive power compared to PI and LPV controllers.

Keywords: *DFIG; Pitch Control; SMC; Torque Control; WECS.*

1. Introduction

The modern wind mills employ doubly fed induction generator (DFIG) for converting the wind energy into electrical energy because of the many advantages of this structure such as reduced size of power electronic converter, flexibility with the variable speed, high energy efficiency and active and reactive power exchange capability in all four quadrants. Because of the fluctuations in the wind velocity from time to time, it is always a concern to control the output power of wind turbine by controlling its speed for different wind velocities. Beyond a specified wind speed limit, the heavy wind gust may damage the blades of wind turbine which causes a reduction in the generation of power. The pitch control is one of the efficient alternative methods for controlling the wind turbine power beyond the rated wind speed and torque control is effective one below the rated wind speed.

A number of torque and pitch controllers such as H∞ control, gain scheduling control, linear parameter varying (LPV) control and model predictive control were proposed in the literature to control the power of the wind turbine. In [1]-[3], the gains of torque and pitch controllers are varied with the variations of wind speed and the internal parameter variations by employing the gain scheduling method. But this method requires accurate wind speed which is not possible because of its measurement at tower rather than the turbine power plant and making practical applications as difficult one [4]. The pitch control design can enhance the performance of DFIG wind turbine by attenuating the disturbances. But this method is not considering the actual disturbances in wind energy conversion system (WECS). Based on differential geometry approach, it is possible to have the linearization of the first order wind power system to obtain variable pitch control [5]. But this model is too simple and gives poor performance because of its simple nature. A multiple model predictive controller [6] is used to obtain the optimum performance near the operating region by the way of continuous control to cope up with the non-linearity of the WECS system. This method is controlling the torque and pitch angle simultaneously for optimum regulation of the wind power while minimizing the torsional fluctuations.

A look up table is implemented in [7] to capture the maximum energy of DFIG for the wind speeds below the rated one through the construction of static torque-speed reference plot. The generator torque controls the speed of WECS under low load conditions and pitch angle control method is employed for full load conditions. The multi objective ∞ control theory is proposed in [8],[9] for the design and control of WECS. But this controller requires the linearization of turbine dynamics about the operating point. The LPV controller based on gain scheduling is proposed in [10] to control the pitch angle and torque together for the entire operating region to maximize the energy capture under both partial and full load conditions. The control algorithm proposed in [11] has multiple objectives such as maximum power point tracking, generator speed control, pitch angle control, maximization of power coefficient under both partial and full load conditions. These objectives are achieved through the torque and pitch control.

The objective of this paper is to design the sliding mode controller (SMC) for the torque and pitch control of WECS to enhance its performance. Section II discusses the mathematical modeling of DFIG based WECS system. Section III presents the design of SMC based torque and pitch controllers. Section IV applies the proposed model and presents simulation results. Section V compares SMC with the LPV and PI controllers applied to WECS system

2. Modeling of DFIG based wind energy control system

The block diagram of DFIG based wind energy control system is shown in Fig. 1. The DFIG is coupled to the wind turbine to capture the wind energy. The power generated by the DFIG is fed to the grid through two ways. One way of feeding the power to the grid from DFIG is through the direct connection of stator of DFIG to the grid and another way is through the two back to back converters connected between the rotor of DFIG and grid. The two back to back converters are called rotor side converter and grid side converter. The rotor side converter is connected to the rotor of DFIG through slip rings and brushes on the rotor side and through the DC link capacitor to the grid side converter. The other side of the grid side converter is connected to the grid through the coupling inductor.

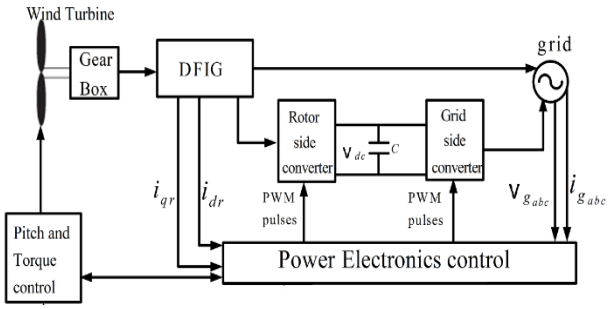

Fig. 1: Block Diagram of DFIG Based Wind Energy Control System.

The power electronic control system interface generates pitch angle command and PWM pulses to the rotor side converter and grid side converter to control the wind turbine power, DC link voltage, active and reactive powers.

a) Modeling of Wind Turbine

The wind turbine blades plays major role in capturing and converting the kinetic energy of the wind to mechanical energy. The power output of WECS is controlled by controlling the pitch angle of the blade or the torque of the generator. The maximum power point depends upon the wind speed and the turbine speed; therefore it is essential to control the speed of the turbine to obtain the maximum power at different wind speeds. The mechanical power output of the wind turbine is given by [12]

$$P_M = \frac{1}{2}\rho A v_w^3 C_p(\lambda,\beta) \tag{1}$$

Where ρ is the density of the air in Kg/m^3, A is the sweep area of the turbine πR^2 in m^2, R is the radius of the turbine blade, v_w is the velocity of wind in m/s, C_p is the power coefficient the turbine blade, λ is the tip speed ratio and β is the pitch angle.

The tip speed ratio is given as

$$\lambda = \frac{\omega_m R}{v_w} \tag{2}$$

Where ω_m is the mechanical speed of the wind turbine.

Modeling of Drive Train

The dynamic behavior of drive train system [13, 14] is represented as

$$T_e - T_w = J\frac{d\omega_m}{dt} + B\omega_m \tag{3}$$

Where J is the total inertia constant of the rotating system, T_e is the electromagnetic torque of DFIG, T_w is mechanical torque applied to the wind turbine rotor extracted from the aerodynamic power and

b) is the friction coefficient of rotational system.

The electromagnetic torque and the electrical speed of the rotor (ω_e) is defined as

$$T_e = \frac{P_{em}}{\omega_m} \tag{4}$$

$$\dot{\omega_e} = \frac{P}{J}\left(\frac{T_w}{N} + T_e\right) \tag{5}$$

$$\omega_e = P\omega_r = PN\omega_m \tag{6}$$

Where P_{em} is the electromagnetic power of the DFIG, ω_r is the DFIG rotor speed, P is the number of pole pairs and N is the gear ratio.

The d-q Axis Model of DFIG

The parks transformation is used to get the stator and rotor voltages of DFIG in d and q axis as in [15] and represented as

$$\begin{cases} v_{ds} = R_s i_{ds} + \omega_s\left((L_s + L_m)i_{qs} + L_m i_{qr}\right) \\ v_{qs} = R_s i_{qs} - \omega_s\left((L_s + L_m)i_{ds} + L_m i_{dr}\right) \\ v_{dr} = R_r i_{dr} + s\omega_s\left((L_r + L_m)i_{qr} + L_m i_{qs}\right) \\ v_{qr} = R_r i_{qr} - s\omega_s\left((L_r + L_m)i_{dr} + L_m i_{ds}\right) \end{cases} \tag{7}$$

where v_{ds}, v_{dr} are d-axis stator and rotor voltages, v_{qs}, v_{qr} are q-axis stator and rotor voltages, i_{ds}, i_{dr} are d-axis stator and rotor currents, i_{qs}, i_{qr} are q-axis stator and rotor currents, R_s, R_r are stator and rotor winding resistances, s is slip, ω_s is synchronous speed, L_s is self inductance of stator, L_r is self inductance of rotor and L_m is the magnetizing inductance.

The voltage equations of (7) can be represented in a matrix form.

$$\begin{bmatrix} v_{ds} \\ v_{qs} \\ v_{dr} \\ v_{qr} \end{bmatrix} = [R^*]\begin{bmatrix} i_{ds} \\ i_{qs} \\ i_{dr} \\ i_{qr} \end{bmatrix} + \frac{d}{dt}\begin{bmatrix} \psi_{ds} \\ \psi_{qs} \\ \psi_{dr} \\ \psi_{qr} \end{bmatrix} + [\omega^*]\frac{d}{dt}\begin{bmatrix} \psi_{ds} \\ \psi_{qs} \\ \psi_{dr} \\ \psi_{qr} \end{bmatrix} \tag{8}$$

$$R^* = \begin{bmatrix} R_s & 0 & 0 & 0 \\ 0 & R_s & 0 & 0 \\ 0 & 0 & R_r & 0 \\ 0 & 0 & 0 & R_r \end{bmatrix} \tag{9}$$

$$\omega^* = \begin{bmatrix} 0 & -\omega & 0 & 0 \\ \omega & 0 & 0 & 0 \\ 0 & 0 & 0 & -(\omega - \omega_r) \\ 0 & 0 & (\omega - \omega_r) & 0 \end{bmatrix} \tag{10}$$

Where ω is the rotating speed of the reference frame set to synchronous speed ω_s.

$$\begin{bmatrix} \psi_{ds} \\ \psi_{qs} \\ \psi_{dr} \\ \psi_{qr} \end{bmatrix} = \begin{bmatrix} L_s & 0 & L_m & 0 \\ 0 & L_s & 0 & L_m \\ L_m & 0 & L_r & 0 \\ 0 & L_m & 0 & L_r \end{bmatrix}\begin{bmatrix} i_{ds} \\ i_{qs} \\ i_{dr} \\ i_{qr} \end{bmatrix} \tag{11}$$

c) Grid Side Converter Control System

The generation of the firing pulses to the grid side converter is shown in Fig. 2. It consists of measuring the capacitor voltage, grid side reactive power, voltage and current. The voltages and currents are transformed to d-q axis for control purpose. The voltage regulator and Var regulator are used to generate the reference currents in the d-q axis. Grid side PI current regulator is used to generate the d-q axis voltages which are then transformed to a-b-c axis quantities to generate the firing pulses to the grid side converter.

d) Rotor Side Converter Control System

The rotor side converter control system is shown in Fig. 3 to generate the firing pulses to the rotor side converter. The rotor side PI current regulator is used to provide the firing pulses to the rotor side converter by extracting the electromagnetic torque, estimated stator flux, reactive power, voltages and currents from the grid. artwork.

Multipliers can be especially confusing. Write "Magnetization (kA/m)" or "Magnetization (10^3 A/m)." Do not write "Magnetization (A/m) × 1000" because the reader would not know whether the top axis label in Fig. 1 meant 16000 A/m or 0.016 A/m. Figure labels should be legible, approximately 8 to 12 point type.

e) Stator Flux Estimator

The estimation of stator flux is shown in Fig. 4 from the d-q axis voltages and currents of the stator of DFIG. The flux linkages of stator in d-q axis are evaluated using the stator voltages, currents and speed given in equations (8-11) which in turn is used to calculate the stator flux.

f) Torque and Pitch Control System

The pitch control system is adopted when the wind speed is greater than the nominal speed and torque control system is implemented for the wind speed less than the nominal speed.

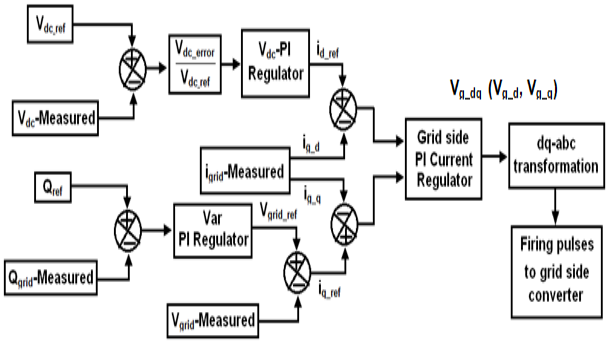

Fig. 2: Grid Side Converter Control System.

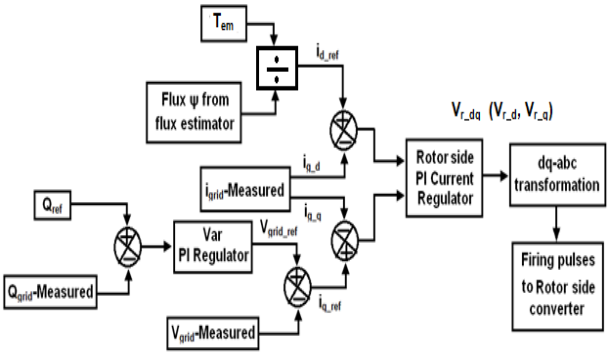

Fig. 3: Rotor Side Converter Control System.

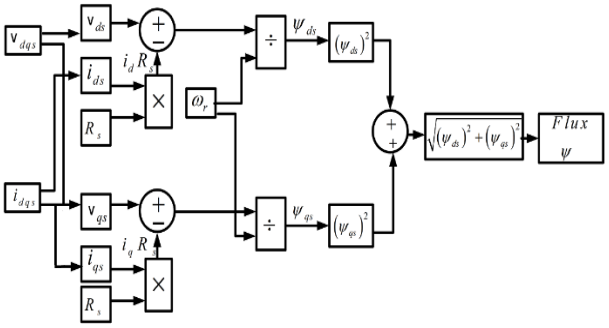

Fig. 4: Stator Flux Estimator.

In the torque control system shown in Fig. 5, the reference torque is obtained from the mechanical rotor speed of DFIG and the measured value of power. The pitch control system shown in Fig. 6 (a) is activated above the rated wind speed to decide the pitch angle. The gain scheduling constant K_p for pitch control system with the gain scheduling is shown in Fig. 6 (b) is evaluated using the equation given in (12).

$$K_{PI} = \begin{cases} 1 \; for -3^0 < \beta \le 0^0 \\ \frac{\beta}{15} + 1 \; for \; 0^0 < \beta \le 30^0 \\ 3 \; for \; \beta > 30^0 \end{cases} \quad (12)$$

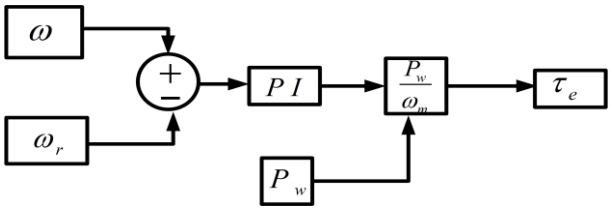

Fig. 5: Torque Control System.

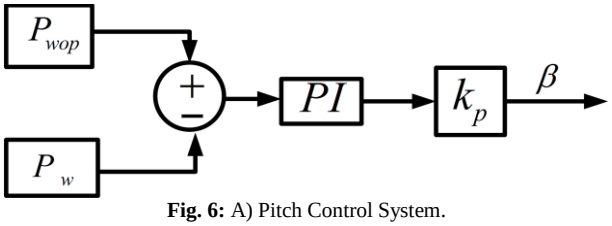

Fig. 6: A) Pitch Control System.

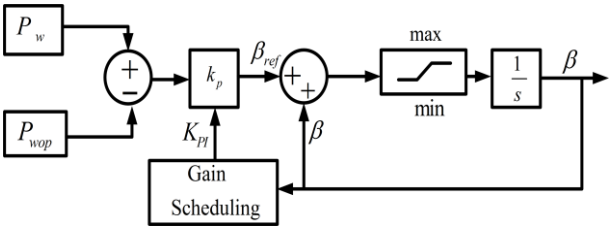

Fig. 6: B) Pitch Control System with the Gain Scheduling.

3. Design of SMC for controlling pitch and torque

The SMC design is carried out in this section for pitch and torque controllers. If the wind speed is above the specific speed, i.e above 25 m/sec, then the wind turbine will not be operated to generate the power. Therefore the pitch angle control system also should be operated up to the specified wind speed beyond which its operation must be ceased to protect the WECS system. The torque control system is implemented when the wind speed is below the rated wind speed.

a) Design of torque controller

The dynamic rotor current equations are obtained by substituting the equations (8)-(11) in the rotor voltage equations (7).

$$\frac{di_{dr}}{dt} = -\frac{R_r}{\sigma} i_{dr} - \frac{L_m}{\sigma L_s}(v_{ds} - R_s i_{ds}) - \omega_r \left(i_{qr} + \frac{L_m}{\sigma L_s}\psi_{qs}\right) + \frac{1}{\sigma} v_{dr} \quad (13)$$

$$\frac{di_{qr}}{dt} = -\frac{R_r}{\sigma} i_{qr} - \frac{L_m}{\sigma L_s}(v_{qs} - R_s i_{qs}) - \omega_r \left(i_{dr} + \frac{L_m}{\sigma L_s}\psi_{ds}\right) + \frac{1}{\sigma} v_{qr} \quad (14)$$

$$where \; \sigma = \frac{L_m^2}{L_s}.$$

The electromagnetic torque of DFIG to be controlled by sliding mode control law is given by

$$T_e = \frac{3PL_m}{2L_s}(i_r \times \psi_s) = \frac{3PL_m}{2L_s}\left(i_{dr} \times \psi_{qs} - i_{qr} \times \psi_{ds}\right) \quad (15)$$

Where

$$\psi_{ds} = \int (v_{ds} - R_s i_{ds}) dt$$
$$\psi_{qs} = \int \left(v_{qs} - R_s i_{qs}\right) dt \quad (16)$$

b) Selection of Sliding Mode Control Law for torque control

The sliding mode surface for electromagnetic torque is chosen as

$$S_{T_e} = e_{T_e} + k_{T_e} \int e_{T_e} dt \quad (17)$$

$$e_{T_e} = T_e^* - T_e \quad (18)$$

Where k_{T_e} represents a positive constant.
The switching function for (17) is selected such that it drives $\boldsymbol{e_{T_e}}$ to zero as in (19).

$$\dot{S_{T_e}} = \left(\dot{T_e^*} - \dot{T_e}\right) + k_{T_e}(T_e^* - T_e) \tag{19}$$

The derivative of the torque equation (15) is given by

$$T_e = \frac{3PL_m}{2L_s}\left(\dot{i_{dr}}\dot{\psi_{qs}} + \dot{\imath_{dr}}\psi_{qs} - i_{qr}\dot{\psi_{ds}} - \dot{\imath_{qr}}\psi_{ds}\right) \tag{20}$$

By substituting (13), (14) and (20) in (19) results as

$$\dot{S_{T_e}} = g_{T_e} - k[a_{11} \quad a_{12}]\begin{bmatrix} v_{dr} \\ v_{qr} \end{bmatrix} \tag{21}$$

Where

$$\begin{gathered} g_{T_e} = g_1\left(i_{dr}, i_{qr}, v_{ds}, v_{qs}, \omega_r, \psi_{dr}, \psi_{qr}, i_{ds}, i_{qs}, e_{T_e}, \dot{T_e}, k_{T_e}\right) \\ a_{11} = P\psi_{qs}, a_{12} = -P\psi_{ds}, k = \frac{3L_m}{2\sigma L_s} \end{gathered} \tag{22}$$

The equivalent control signals assumed to move toward the zero sliding surface is written as

$$\begin{bmatrix} v_{dr_{eq}} \\ v_{qr_{eq}} \end{bmatrix} = \frac{B^{-1}}{k} g_{T_e} \tag{23}$$

Where

$$B = [a_{11} \quad a_{12}]$$

By substituting (23) in (21) results as

$$\dot{S_{T_e}} = 0 = \dot{e_{T_e}} + k_{T_e} e_{T_e} \tag{24}$$

The equation (24) indicates that the error is approaching zero with the control signals $v_{dr_{eq}}$ and $v_{qr_{eq}}$. But these control signals have to be modified for the deviations in the parameters of DFIG. The varying parameters of DFIG are compensated by introducing the compensation variables v_{dr_c} and v_{qr_c}.

$$\begin{aligned} v_{dr} &= v_{dr_{eq}} + v_{dr_c} \\ v_{qr} &= v_{qr_{eq}} + v_{qr_c} \end{aligned} \tag{25}$$

v_{dr_c} and v_{qr_c} are defined as

$$\begin{bmatrix} v_{dr_c} \\ v_{qr_c} \end{bmatrix} = B^{-1} c_{T_e} sgn S_{T_e} \tag{26}$$

Where c_{T_e} is a positive constant.
After introducing the compensation variables, the equation (21) is rewritten as

$$\dot{S_{T_e}} = g_{T_e} - kB\begin{bmatrix} v_{dr} \\ v_{qr} \end{bmatrix} + d_{r2} \tag{27}$$

Where d_{r2} is the term that represents non-linearity due to discontinuous control action that happens internally. By substituting the equation (23), (25) and (26) in the equation (27), the derivative of sliding mode surface equation is rewritten as

$$\dot{S_{T_e}} = kc_{T_e} sgn(S_{T_e}) + d_{r2} \tag{28}$$

Lyapunov function is chosen for the verification convergence condition of equations (23), (25) and (26) as given below.

$$V = \frac{1}{2} S_{T_e}^T S_{T_e} \geq 0 \tag{29}$$

To satisfy the convergence condition, the equation (21) must be negative definite, i.e.

$$\dot{V} = \frac{1}{2} S_{T_e}^T \dot{S_{T_e}} \leq 0 \tag{30}$$

Substitution of (28) in (30) gives

$$\dot{V} = S_{T_e} kc_{T_e} sgn\left(S_{T_e}\right) + S_{T_e} d_{r2} \leq 0 \tag{31}$$

The equation (31) converges to zero, if it satisfies the following condition.

$$c_{T_e} \gg \frac{|d_{r2}|}{B} \tag{32}$$

Due to the sign function in (26), the control is not continuous. In order to achieve the continuous control, the equation (26) is modified after allowing it to pass through the low pass filter.

$$\begin{aligned} \begin{bmatrix} v_{dr_c} \\ v_{qr_c} \end{bmatrix} &= B^{-1} v_{Tav} \\ v_{Tav}(s) &= \frac{1}{1+sT} v_{T1}(s) \end{aligned} \tag{33}$$

Where T is the time constant of low pass filter.
Finally the control signal obtained from (23), (25) and (33) is as follows.

$$\begin{bmatrix} v_{dr} \\ v_{qr} \end{bmatrix} = B^{-1} g_{T_e} + B^{-1}\, v_{Tav} \tag{34}$$

The equation (34) makes torque control as robust to the system parameter variations.

c) Design of Pitch Controller

The schematic diagram of pitch control system for DFIG based WECS system is shown in Fig. 7. The pitch angle control system processes the error between the generator output power (P_g) and the reference power (P_{wop}) and current pitch angle β to generate β_{eq}. If SMC is employed for pitch angle control system, β_{eq} is discontinuous. To make β_{eq} as continuous, it is allowed to pass it through the low pass filter and is given as input to WECS system.

d) Selection of Sliding Mode Control Law for Pitch Control

Fig. 8 shows the implementation of SMC for pitch control system. The sliding mode surface chosen for pitch control system is

$$S_p = e_p + k_p \int e_p dt \tag{35}$$

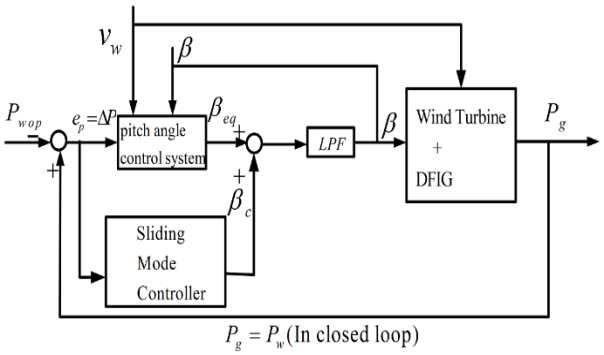

Fig. 7: The Schematic Diagram of Pitch Control System.

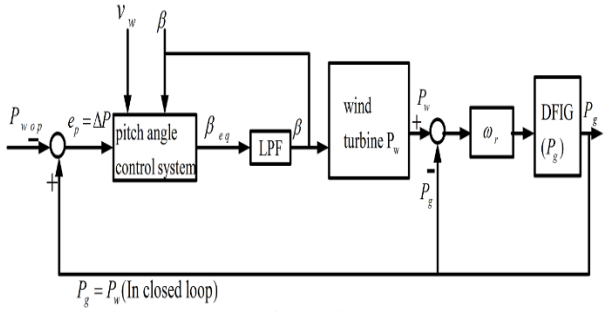

Fig. 8: Implementation of SMC for Pitch Control System.

The linearization of power error (e_p) equation is written as

$$e_p = \Delta P = P_w - P_{wop} = \frac{\partial P_w}{\partial v_w}\Delta v_w + \frac{\partial P_w}{\partial \beta}\Delta\beta = \zeta \Delta v_w + \xi \Delta\beta \quad (36)$$

Where

$$\frac{\partial P_w}{\partial v_w} = \zeta \; and \; \frac{\partial P_w}{\partial \beta} = \xi$$

The objective of the control system is to drive the error e_p to zero by selecting the switching function as

$$\dot{S_p} = \left(\dot{P_w} - \dot{P_{wop}}\right) + k_p(P_w - P_{wop}) \quad (37)$$

As in [16], $\dot{\boldsymbol{P_w}}$ is represented as

$$\begin{aligned} \dot{P_w} &= \dot{a_1}(\beta) + \dot{a_2}(\beta)v_w^2 \\ \dot{a_1}(\beta) &= a_{12} + 2a_{13}\beta + 3a_{14}\beta^2 \\ \dot{a_2}(\beta) &= a_{22} + 2a_{23}\beta + 3a_{24}\beta^2 \end{aligned} \quad (38)$$

Substituting equation (1) and (38) in (37) results as

$$\dot{S_p} = f_p + H[\beta] \quad (39)$$

Where

$$f_p = (C_p, \omega_r, P_{wop}, \dot{k}_p, e_p)$$
$$H = \frac{\rho A}{2}$$

The equivalent control signal in (39) is assumed as

$$[\beta_{eq}] = H^{-1} f_p \quad (40)$$

Substitution of (40) in (39) yields

$$\dot{S_p} = 0 = \dot{e_p} + k_p e_p \quad (41)$$

The equation (41) shows that the control variable drives the error towards zero. But the control signals have to be modified with the changes in the dynamics of aerodynamic wind turbine. To incorporate the changes in control signals to compensate these dynamics, the compensation control signal β_c is added to the equivalent control signal β_{eq}.

$$\beta = \beta_{eq} + \beta_c \quad (42)$$

$$[\beta_c] = H^{-1} k_{pc} sgn(S_p) \quad (43)$$

Where k_{pc} is a positive constant. After incorporating the non linear term d_{r1} due to the stochastic variations of wind speed, the equation (39) is rewritten as

$$\dot{S_p} = f_p + H[\beta] + d_{r1} \quad (44)$$

By substituting (40), (42) and (43) in (44), the switching function is represented as

$$\dot{S_p} = H k_{pc} sgn(S_p) + d_{r1} \quad (45)$$

To verify the convergence of switching variable, consider the Lyapunov function as

$$V = \frac{1}{2} S_p^T S_p \geq 0 \quad (46)$$

To satisfy the convergence condition, the equation (46) must be negative definite, i.e.

$$\dot{V} = \frac{1}{2} S_p^T \dot{S_p} \leq 0 \quad (47)$$

Substitution of (45) in (47) gives

$$\dot{\mathrm{V}} = \mathrm{S_p H k_{pc} sgn}(\mathrm{S_p}) + \mathrm{S_p d_{r1}} \leq 0 \quad (48)$$

The equation (31) converges to zero, if it satisfies the following condition.

$$\mathrm{k_{pc}} \gg \frac{|\mathrm{d_{r1}}|}{\mathrm{H}} \quad (49)$$

Due to the sign function in (43), the control is not continuous. In order to achieve the continuous control the equation (43) is modified after allowing it to pass through the low pass filter.

$$\begin{aligned} [\beta_c] &= \mathrm{H^{-1} v_{pav}} \\ \mathrm{v_{pav}(s)} &= \frac{1}{1+sT}\mathrm{v_{p1}(s)} \end{aligned} \quad (50)$$

Where T is the time constant of low pass filter.
Finally the control signal obtained from (40), (42) and (50) is as follows.

$$\beta = \mathrm{H^{-1} f_p} + \mathrm{H^{-1}\, v_{pav}} \quad (51)$$

The equation (50) makes pitch control as robust to the non linear dynamics of wind turbine.

4. Simulation of DFIG based WECS

The wind energy control system with SMC for torque and pitch control is modeled in MATLAB/SIMULINK and its dynamics are simulated. The parameters of the simulation model are given in table 1.

Table 1: DFIG Based WECS Simulation Parameters

Wind Turbine and Rotor	
Number of turbine blades	3
Cut out speed of turbine	25 m/sec
Cut in speed of turbine	3 m/sec
Rated speed of turbine	12 m/sec
tip speed ratio	8
Density of air	1.25 Kg/m^3
Power coefficient	0.49
Maximum speed of rotor	23 rpm
Rated speed of rotor	22 rpm
Blade radius	40m
Drive Train	
Turbine inertia	90×10^6 kg-m^2/rad
Spring constant of turbine	160×10^6 N-m/rad
Damping constant of turbine	10×10^6 N-m/rad/sec
Gear ratio	250:3
Pitch actuator	
Time constant	0.1 sec
Minimum/maximum pitch angle	$0^0/90^0$
Minimum/maximum pitch rate	$-8^0/8^0$per sec
Supply frequency	60 Hz
Number of pole pairs	2

DFIG	
Rated power	3 kW
Rated speed of generator	1800 rpm
Inertia of Generator	60 kg-m^2/rad
Generator torque	13.4 KN-m

The rated wind speed is taken as 12 m/s while the average wind speed increases from 11 m/s to 14 m/s and then maintained above the rated value with the 8 % of wind turbulence intensity. The maximum rate of pitch angle is limited to 8 deg/s. The results are presented in two regions, one is below the rated generator speed (ωg*) and another one is above the rated generator speed. In the region (ωg≤ ωg*), the generator power is maximized using the torque controller, while the torque and pitch controllers are operated in harmony to control the inlet power of DFIG. The simulation results are plotted in figures 9-21, for wind speed, torque, generated power, three phase voltage and current at stator terminals, rotor speed, frequency at the stator terminals and pitch angle.

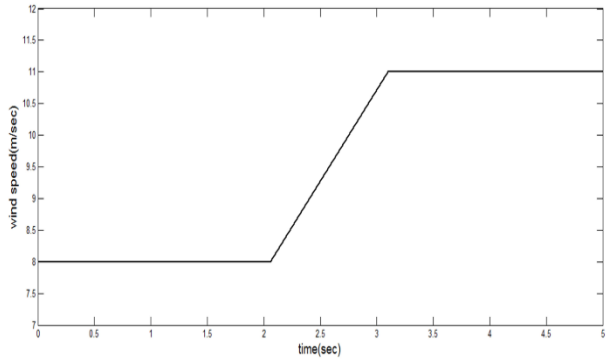

Fig. 9: wind speed vs time.

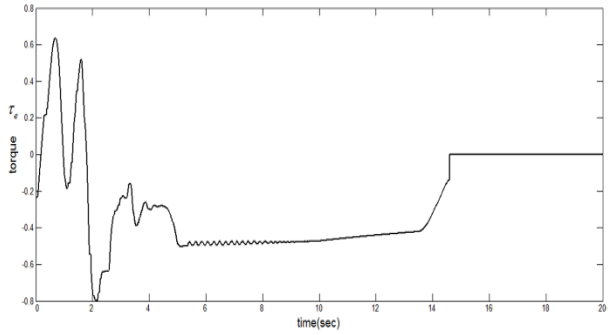

Fig. 10: Torque vs time.

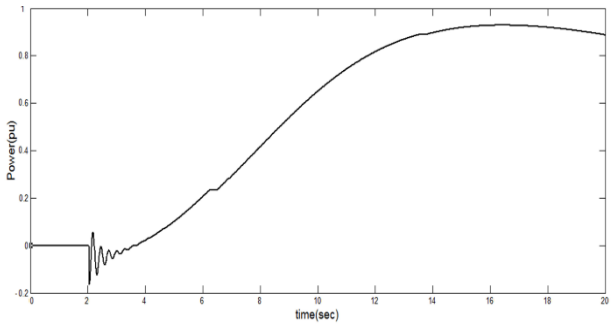

Fig. 11: Active Power of DFIG vs Time.

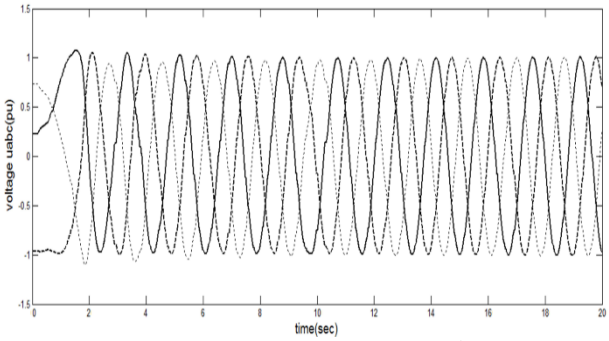

Fig. 12: Three-Phase Voltage at Stator Terminals of DFIG vs Time.

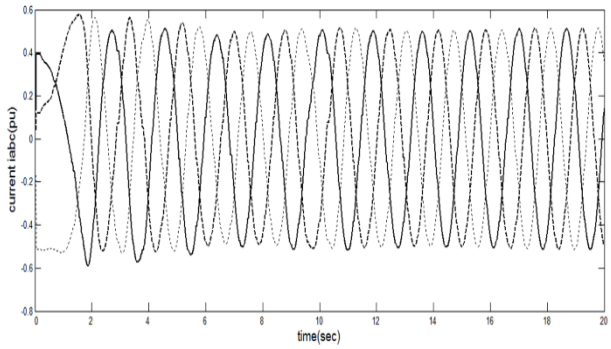

Fig. 13: Three Phase Current at Stator Terminals vs Time.

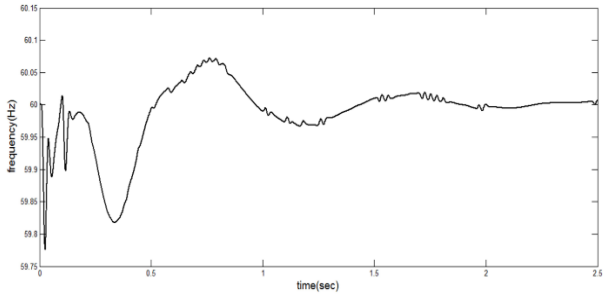

Fig. 14: Rotor Speed of DFIG vs Time.

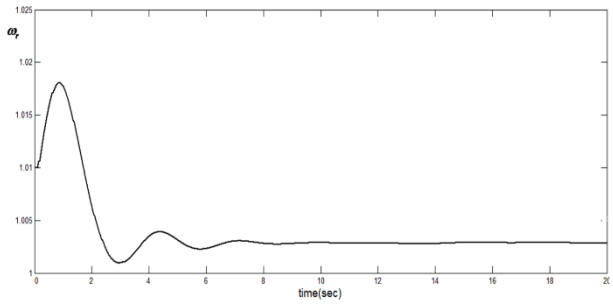

Fig. 15: Frequency at Stator Terminals vs Time.

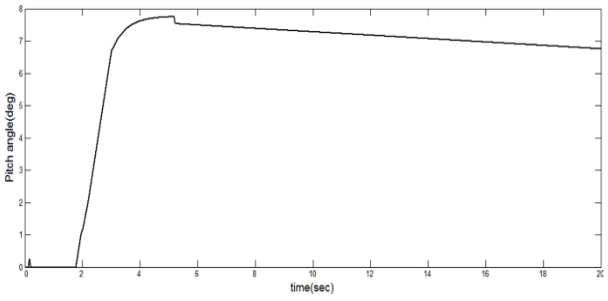

Fig. 16: Pitch Angle vs Time.

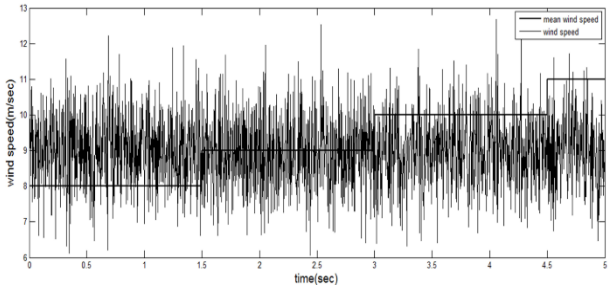

Fig. 17: Wind vs Time Profile with Turbulence.

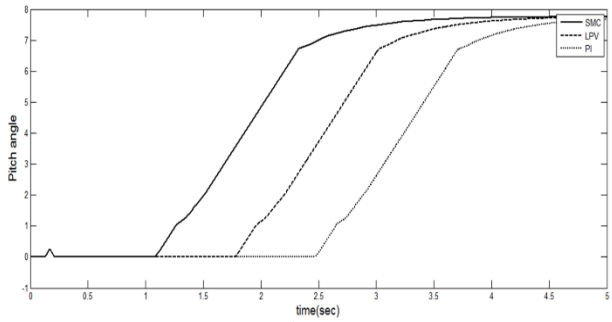

Fig. 18: Pitch Angle vs Time for SMC, LPV and PI Controllers.

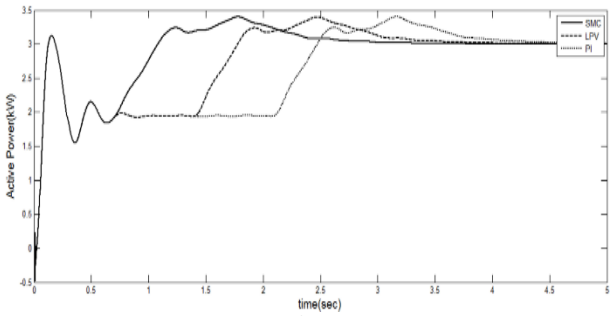

Fig. 19: Active Power vs Time for SMC, LPV and PI Controllers.

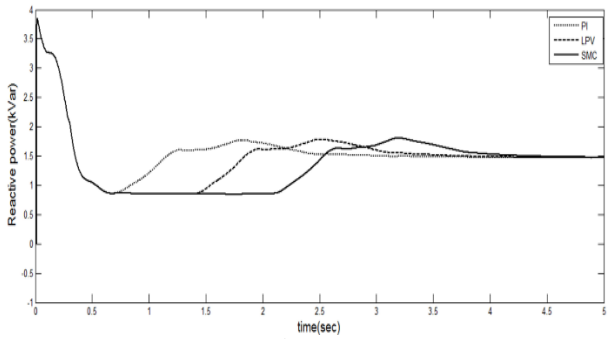

Fig. 20: Reactive Power Vs Time for SMC, LPV and PI Controllers.

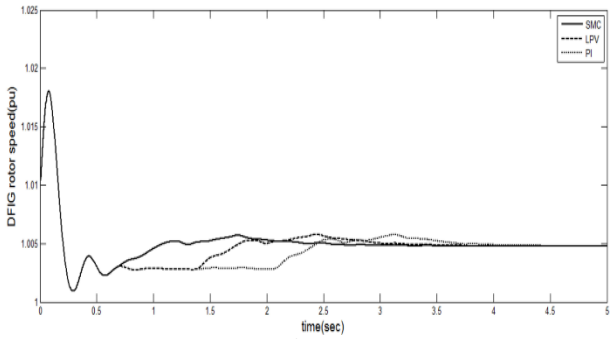

Fig. 21: Rotor Speed vs Time for SMC, LPV and PI Controllers.

5. Results and discussion

Fig. 9 shows the wind speed variation with time while the fig.17 shows the wind speed with time for wind turbulence intensity of 8%. The wind speed is varying from 8 to 11 m/sec from t=2 sec to 3.3 sec and there after maintained constant. Fig. 10 shows the variation of the torque with time for the wind speed fluctuations. It is observed that the torque is -0.8 pu at t=2 sec. when the wind speed is increasing from t=2 sec, abrupt torque pulsations are observed upto 3.3 sec and finally settled to 0 pu at 15 sec when the generator speed is almost reached the rated speed. Fig. 11 shows the generator power with time in which the power pulsations are observed from t=2 to 3.3 sec during the increase of wind speed and generating steady state power of 1 pu at 15 sec at the rated speed of the generator. In the graphs of three phase voltage (Fig. 12) and current (Fig. 13) at stator terminals, rotor speed (Fig. 14) and frequency (Fig. 15) at the stator terminals, the transients are observed up to t=2 sec. Fig. 16 shows the variation of the pitch angle with time, where there is a steady change of pitch angle from 0 to 8 degrees during the maximization of the generator power up to 5 sec and settled at the pitch angle of 7 degrees once the transients are over. Therefore the Figures 9-15 indicate that the transients are suppressed after a long time of 15 sec. By employing the SMC based torque and pitch controllers, the time duration of the transients are reduced to enable the parameters to reach the steady state values quickly at almost 3.3 sec.

The simulation results shown in Figures 18-21 depict that the SMC is successfully implemented in controlling the inlet power of DFIG and suppress the transients quickly. In figures 19 and 20, the active and reactive powers with time are shown for three controllers of SMC, LPV and PI. It is observed that SMC controller makes the active power to attain the maximum value very quickly compared to LPV and PI controllers. Fig. 21 shows the rotor speed of DFIG with time in which the SMC is much better than LPV and PI controllers in controlling the speed of DFIG. When the speed is above the nominal speed, SMC is acting in superior manner in controlling the pitch angle compared to LPV and PI controllers as shown in Fig. 18.

6. Conclusion

The torque and pitch control of Wind Energy Conversion System (WECS) is modeled using MATLAB/SIMULINK environment and simulations are carried out with three controllers of SMC, LPV and PI. The detailed analysis of SMC controller with torque and pitch control mechanism along the verification of convergence condition by Lyupunov stability are presented. The performance parameters such as pitch angle, active power, reactive power and rotor speed are compared for the Proportional plus Integral (PI), Linear Parameter Varying (LPV) and SM control schemes. Simulation results exhibit that the performance of SM control is superior in terms of pitch, speed, active and reactive power compared to PI and LPV controllers.

References

[1] . Y. Z. F. Lescher and P. Borne, “Robust gain scheduling controller for pitch regulated variable speed wind turbine,” Stud. Inform. Control, vol. 14, no. 12, pp. 299–315, 2005.

[2] R. M. F. Bianchi and C. Christiansen, “Gain scheduling control of variable speed wind energy conversion systems using quasi-PV models,” Control Engg. Practice, vol. 13, no. 2, pp. 247–255, 2005.

[3] D. Leith and W. Leithead, “Appropriate realisation of gain-scheduled controllers with application to wind turbine regulation,” Int. J. Control, vol. 65, no. 2, pp. 223–248, 2005.

[4] B. K. Stol, B. Rigney, “Accommodating control of a variable-speed turbine using a symbolic dynamics structural model,” Proc. 2000 ASME Wind Energy Symp.

[5] J. W. X.Y. Zhang and J.-M. Yang, “H-infinity robust control of constant power out- put for the wind energy conversion system above rated wind,” Control Theory and Application, vol. 25, no. 2, pp. 321–324, 2008.

[6] D. W. M. Soliman, O.P. Malik, “Multiple model multiple-input multiple-output predictive control for variable speed variable pitch wind energy conversion systems,” IET Renew. Power Gener., vol. 5, no. 2, p. 124136, 2011.

[7] H. D. B. Fernando A. Inthamoussou, Fernando D. Bianchi and R. J. Mantz, "LPV wind turbine control with anti-windup features covering the complete wind speed range," IEEE Trans. on Energy Conversion, vol. 29, no. 1, pp. 259–266, 2014.
[8] A.U. Endusa Billy Muhando, Tomonobu Senjyu and T. Funabashi, "Gain-scheduled H∞ control for WECS via LMI techniques and parametrically dependent feedback part i: Model development fundamentals," IEEE Trans. on Industrial Electronics, vol. 58, no. 1, pp. 48–56, 2011.
[9] U. Endusa Billy Muhando, Tomonobu Senjyu and T. Funabashi, "Gain-scheduled H∞ control for WECS via LMI techniques and parametrically dependent feedback part ii: Controller design and implementation," IEEE Trans. on Industrial Electronics, vol. 58, no. 1, pp. 57–65, 2011.
[10] O. P. M. Mostafa Soliman, Member and D. T. Westwick, "Multiple model predictive control for wind turbines with doubly fed induction generators," IEEE Trans on Sustainable Energy, vol. 2, no. 3, pp. 215–225, 2011.
[11] T. D. Z. J. Can Huang, Fangxing Li and X. Ma, "Second-order cone programming-based optimal control strategy for wind energy conversion systems over complete operating regions," IEEE Trans. on Sustainable Energy, vol. 6, no. 1, pp. 263–271, 2015.
[12] S. Heier, Grid Integration of Wind Energy Conversion Systems. ISBN 0-97143-X: John Wiley and Sons Ltd, 1998.
[13] Brice Beltran and M. E. H. Benbouzid, "Sliding mode power control of variable-speed wind energy conversion systems," IEEE Trans. on Energy Conversion, vol. 23, no. 2, pp. 551–558, 2008.
[14] Brice Beltran, Tarek Ahmed-Ali and M. E. H. Benbouzid, "High-order sliding control of variable speed wind turbines," IEEE Trans. On Industrial Electronics, vol. 56, no. 9, pp. 3314–3321, 2009.
[15] M. S.Chondrogiannis, "Stability of double fed induction generator under stator voltage oriented vector control," IET Renewable Power Generation, vol. 2, no. 3, pp. 170–180, 2008.
[16] G. T. L. X. Miren Itsaso Martinez, Ana Susperregui, "Sliding-mode control of a wind turbine-driven double-fed induction generator under non-ideal grid voltages," IET Renewable Power Generation, vol. 7, no. 4, pp. 370–379, 2013.